J|A|C|S
ARTICLES
Published on Web 09/30/2006

Direct UV Raman Monitoring of 3_{10}-Helix and π-Bulge Premelting during α-Helix Unfolding

Aleksandr V. Mikhonin and Sanford A. Asher*

Contribution from the Department of Chemistry, University of Pittsburgh, Pittsburgh, Pennsylvania 15260

Received April 3, 2006; E-mail: asher@pitt.edu

Abstract: We used UV resonance Raman (UVRR) spectroscopy exciting at ~200 nm within the peptide bond $\pi \rightarrow \pi^*$ transitions to selectively study the amide vibrations of peptide bonds during α-helix melting. The dependence of the amide frequencies on their Ψ Ramachandran angles and hydrogen bonding enables us, for the first time, to experimentally determine the temperature dependence of the peptide bond Ψ Ramachandran angle population distribution of a 21-residue mainly alanine peptide. These Ψ distributions allow us to easily discriminate between α-helix, 3_{10}-helix and π-helix/bulge conformations, obtain their individual melting curves, and estimate the corresponding Zimm and Bragg parameters. A striking finding is that α-helix melting is more cooperative and shows a higher melting temperature than previously erroneously observed. These Ψ distributions also enable the experimental determination of the Gibbs free energy landscape along the Ψ reaction coordinate, which further allows us to estimate the free energy barriers along the AP melting pathway. These results will serve as a benchmark for the numerous untested theoretical studies of protein and peptide folding.

Introduction

The formation and melting of α-helices are the most fundamental secondary structure dynamics of peptides and proteins in their conformational search between their folded and unfolded structures. This conformational search has been studied for well over 50 years. The basic theory, which modeled this transition was proposed by Zimm and Bragg[1] and Poland and Sheraga[2] approximately forty-five years ago, envisioned a transition between an ordered α-helix structure and a disordered random coil structure. Cooperativity in the transition was modeled through the assumption that the nucleation step for α-helix formation occurs at a higher free energy because of the entropic expense associated with restricting four amino acid residues to occur in α-helical conformation prior to compensation by the intrahelix hydrogen bonding.

This theory, which appeared to adequately model α-helix stability is parametrized in terms of three parameters, σs, the small nucleation parameter, s the propagation parameter, and N the length of the peptide. Experimental studies of typical synthetic peptides which form α-helices (such as peptides rich in ala) indicate that the α-helix melting and formation is only weakly cooperative, with melting temperatures of between 10 and 30 °C.[3−7] Recent kinetic α-helix melting studies, which have utilized pump−probe spectroscopic techniques such as temperature-jump fluorescence, IR, and UV Raman investigations often demonstrate single-exponential melting.[3−6,8] More complex multiexponential and/or nonexponential behavior is also sometimes observed,[7,9,10] as are different kinetics for T-jumps between different initial and final temperatures. IR studies of peptides isotopically labeled at specific positions, also indicate that the different parts of polypeptide chains have different melting rates.[11,12] The time scale for melting appears to be ~200 ns, a long time compared to the sub-nsec expected propagation times required to add or remove individual α-helical residues at the α-helix ends.

Recent molecular dynamics (MD) simulations of α-helix conformational dynamics have demonstrated that α-helix melting and formation is likely to be complex,[13−19] since the other

(1) Zimm, B. H.; Bragg, J. K. *J. Chem. Phys.* **1959**, *31*, 526−535.
(2) Poland, D.; Scheraga, H. A. *J. Chem. Phys.* **1966**, *45*, 2071−2090.
(3) Williams, S.; Causgrove, T. P.; Gilmanshin, R.; Fang, K. S.; Callender, R. H.; Woodruff, W. H.; Dyer, R. B. *Biochemistry* **1996**, *35*, 691−697.
(4) Thompson, P. A.; Munoz, V.; Jas, G. S.; Henry, E. R.; Eaton, W. A.; Hofrichter, J. *J. Phys. Chem. B* **2000**, *104*, 378−389.
(5) Lednev, I. K.; Karnoup, A. S.; Sparrow, M. C.; Asher, S. A. *J. Am. Chem. Soc.* **1999**, *121*, 8074−8086.
(6) Lednev, I. K.; Karnoup, A. S.; Sparrow, M. C.; Asher, S. A. *J. Am. Chem. Soc.* **2001**, *123*, 2388−2392.
(7) Huang, C.-Y.; Klemke, J. W.; Getahun, Z.; DeGrado, W. F.; Gai, F. *J. Am. Chem. Soc.* **2001**, *123*, 9235−9238.
(8) Werner, J. H.; Dyer, R. B.; Fesinmeyer, R. M.; Andersen, N. H. *J. Phys. Chem. B* **2002**, *106*, 487−494.
(9) Bredenbeck, J.; Helbing, J.; Kumita, J. R.; Woolley, G. A.; Hamm, P. *Proc. Natl. Acad. Sci. U.S.A.* **2005**, *102*, 2379−2384.
(10) Huang, C.-Y.; Getahun, Z.; Zhu, Y.; Klemke, J. W.; DeGrado, W. F.; Gai, F. *Proc. Natl. Acad. Sci. U.S.A.* **2002**, *99*, 2788−2793.
(11) Ramajo, A. P.; Petty, S. A.; Starzyk, A.; Decatur, S. M.; Volk, M. *J. Am. Chem. Soc.* **2005**, *127*, 13784−13785.
(12) Decatur, S. M. *Acc. Chem. Res.* **2006**, *39*, 169−175.
(13) Hummer, G.; Garcia, A. E.; Garde, S. *Phys. Rev. Lett.* **2000**, *85*, 2637−2640.
(14) Ferrara, P.; Apostolakis, J.; Caflisch, A. *J. Phys. Chem. B* **2000**, *104*, 5000−5010.
(15) Sorin, E. J.; Pande, V. S. *Biophys. J.* **2005**, *88*, 2472−2493.
(16) Bertsch, R. A.; Vaidehi, N.; Chan, S. I.; Goddard, W. A., III. *Proteins* **1998**, *33*, 343−357.
(17) Levy, Y.; Jortner, J.; Becker, O. M. *Proc. Natl. Acad. Sci. U.S.A.* **2001**, *98*, 2188−2193.
(18) Irbaeck, A.; Mohanty, S. *Biophys. J.* **2005**, *88*, 1560−1569.
(19) DiCapua, F. M.; Swaminathan, S.; Beveridge, D. L. *J. Am. Chem. Soc.* **1990**, *112*, 6768−6771.

states such as turns, 3_{10}-, and π-helices are involved as the α-helix conformation nucleates, grows, and melts.[20−32] These MD studies suggest that these 3_{10} and π helical conformations, as well as different turn motifs, are intermediates in α-helix formation and melting, and can also be present as defects in long α-helices.

A number of recent experimental α-helix melting studies have begun to challenge the standard view of the α-helix conformational dynamics discussed above. A major challenge is the clear recent demonstrations that α-helices do not melt to random coil conformations.[33−37] Rather, the unfolded peptides and proteins exist in PPII conformations,[33−50] which consist of left-handed helices with 3 residues per helical turn, where the peptide bonds hydrogen-bond to water.[51−53]

In the work here, we utilize UV resonance Raman (UVRR) spectroscopy with excitation within the peptide bond $\pi \rightarrow \pi^*$ transitions[54] to selectively probe the vibrational spectra of the peptide bonds.[55−58] Our recent examination of the UVRR spectra of peptides and proteins has uncovered a quantitative correlation between the frequency of a particular vibrational band called the amide III_3 ($AmIII_3$) band and the peptide bond Ramachandran Ψ angle.[59] This quantitative correlation enables the direct experimental monitor of motion along the major reaction coordinate for secondary structure evolution. Here, we utilize this correlation to quantitatively monitor the different secondary structures involved in α-helix melting and how they evolve with temperature. This enables us for the first time to monitor both the change in average α-helical length and the presence of non α-helical defects.

Experimental Section

Materials. The 21-residue alanine-based peptide AAAAA(AAARA)$_3$A (AP, also called Fs) was prepared (HPLC pure) at the Pittsburgh Peptide Facility by using the solid-state peptide synthesis method. The AP solutions in water contained 3 mg/mL concentrations of AP, and 0.2 M concentrations of sodium perchlorate, which was used as internal intensity and frequency standards. All UVRR spectra were normalized to the intensity of the ClO_4^- Raman band (932 cm^{-1}).

UV Resonance Raman Instrumentation. The UVRR apparatus is described in detail by Bykov et al.[60] and Lednev et al.[5] Briefly, the third harmonic of a Coherent Infinity Nd:YAG laser operating at 100 Hz with a 3 ns pulse width was Raman shifted by five anti-Stokes harmonics in 40 psi hydrogen gas to 204 nm to excite the amide band UVRR spectra. The Raman scattered light was collected at an angle close to backscattering and was dispersed with a partially subtractive double monochromator. The Raman scattered light was detected by using a Princeton Instruments Spec-10:400B CCD camera purchased from Roper Scientific. The spectral accumulation times were ∼15 min with a spectral resolution of ∼10 cm^{-1}.

Results and Discussion

UVRR α-Helix-like $AmIII_3$ Band Dramatically Narrows at Elevated Temperatures. Figure 1 shows the temperature dependence of the 204 nm-excited UVRR spectra of a 21 amino acid residue mainly ala peptide, AP, containing three arg for solubility. This peptide is >55% α-helical at 0 °C and less than 10% α-helical by 50 °C.[5,6] At 50 °C, the peptide is predominantly in the PPII conformation.[34]

The measured UVRR spectra at different temperatures are shown in Figure 1A, while Figure 1B shows spectra of the pure PPII conformation at different temperatures. The 49 and 65 °C Figure 1A spectra are essentially pure PPII spectra, while the lower temperature spectra are a mixture of PPII and α-helix-like spectra.

We previously[5] calculated the underlying pure PPII spectra at different temperatures, as shown in Figure 1B. Originally, we incorrectly denoted these spectra as "random coil",[5] but later showed that these are essentially pure PPII spectra, although minor contributions from various turns and β-strand conformations could also exist.[34] The major temperature induced spectral differences in the PPII spectra derive from small frequency shifts owing to the decreased peptide bond−water hydrogen bond strength as the temperature increases.[34,38,61] Figure 1C−F difference spectra at different temperatures, which were calculated by subtracting off the PPII spectral contributions, look α-helix-like,[5] but contain additional features.

(20) Young, W. S.; Brooks, C. L., III. *J. Mol. Biol.* **1996**, *259*, 560−572.
(21) Shirley, W. A.; Brooks, C. L., III. *Proteins* **1997**, *28*, 59−71.
(22) Doruker, P.; Bahar, I. *Biophys. J.* **1997**, *72*, 2445−2456.
(23) Takano, M.; Yamato, T.; Higo, J.; Suyama, A.; Nagayama, K. *J. Am. Chem. Soc.* **1999**, *121*, 605−612.
(24) Sorin, E. J.; Rhee, Y. M.; Shirts, M. R.; Pande, V. S. *J. Mol. Biol.* **2006**, *356*, 248−256.
(25) Armen, R.; Alonso, D. O. V.; Daggett, V. *Protein Sci.* **2003**, *12*, 1145−1157.
(26) Freedberg, D. I.; Venable, R. M.; Rossi, A.; Bull, T. E.; Pastor, R. W. *J. Am. Chem. Soc.* **2004**, *126*, 10478−10484.
(27) Lee, K.-H.; Benson, D. R.; Kuczera, K. *Biochemistry* **2000**, *39*, 13737−13747.
(28) Zhang, W.; Lei, H.; Chowdhury, S.; Duan, Y. *J. Phys. Chem. B* **2004**, *108*, 7479−7489.
(29) Huo, S.; Straub, J. E. *Proteins* **1999**, *36*, 249−261.
(30) Mahadevan, J.; Lee, K.-H.; Kuczera, K. *J. Phys. Chem. B* **2001**, *105*, 1863−1876.
(31) Tirado-Rives, J.; Maxwell, D. S.; Jorgensen, W. L. *J. Am. Chem. Soc.* **1993**, *115*, 11590−11593.
(32) Wang, Y.; Kuczera, K. *J. Phys. Chem. B* **1997**, *101*, 5205−5213.
(33) Mezei, M.; Fleming, P. J.; Srinivasan, R.; Rose, G. D. *Proteins* **2004**, *55*, 502−507.
(34) Asher, S. A.; Mikhonin, A. V.; Bykov, S. B. *J. Am. Chem. Soc.* **2004**, *126*, 8433−8440.
(35) Garcia, A. E. *Polymer* **2004**, *45*, 669−676.
(36) Shi, Z.; Woody, R. W.; Kallenbach, N. R. *Adv. Protein Chem.* **2002**, *62*, 163−240.
(37) Blanch, E. W.; Morozova-Roche, L. A.; Cochran, D. A. E.; Doig, A. J.; Hecht, L.; Barron, L. D. *J. Mol. Biol.* **2000**, *301*, 553−563.
(38) Mikhonin, A. V.; Myshakina, N. S.; Bykov, S. V.; Asher, S. A. *J. Am. Chem. Soc.* **2005**, *127*, 7712−7720.
(39) McColl, I. H.; Blanch, E. W.; Hecht, L.; Kallenbach, N. R.; Barron, L. D. *J. Am. Chem. Soc.* **2004**, *126*, 5076−5077.
(40) Syme, C. D.; Blanch, E. W.; Holt, C.; Jakes, R.; Goedert, M.; Hecht, L.; Barron, L. D. *Eur. J. Biochem.* **2002**, *269*, 148−156.
(41) Smyth, E.; Syme, C. D.; Blanch, E. W.; Hecht, L.; Vasak, M.; Barron, L. D. *Biopolymers* **2001**, *58*, 138−151.
(42) Blanch, E. W.; Gill, A. C.; Rhie, A. G. O.; Hope, J.; Hecht, L.; Nielsen, K.; Barron, L. D. *J. Mol. Biol.* **2004**, *343*, 467−476.
(43) Shi, Z.; Olson, C. A.; Rose, G. D.; Baldwin, R. L.; Kallenbach, N. R. *Proc. Natl. Acad. Sci. U.S.A.* **2002**, *99*, 9190−9195.
(44) Creamer, T. P.; Campbell, M. N. *Adv. Prot. Chem.* **2002**, *62*, 263−282.
(45) Rucker, A. L.; Creamer, T. P. *Protein Sci.* **2002**, *11*, 980−985.
(46) Chellgren, B. W.; Creamer, T. P. *Biochemistry* **2004**, *43*, 5864−5869.
(47) Liu, Z.; Chen, K.; Ng, A.; Shi, Z.; Woody, R. W.; Kallenbach, N. R. *J. Am. Chem. Soc.* **2004**, *126*, 15141−15150.
(48) Adzhubei, A. A.; Sternberg, M. J. E. *J. Mol. Biol.* **1993**, *229*, 472−493.
(49) Pappu, R. V.; Rose, G. D. *Prot. Sci.* **2002**, *11*, 2437−2455.
(50) Rath, A.; Davidson, A. R.; Deber, C. M. *Biopolymers* **2005**, *80*, 179−185.
(51) Fleming, P. J.; Fitzkee, N. C.; Mezei, M.; Srinivasan, R.; Rose, G. D. *Prot. Sci.* **2005**, *14*, 111−118.
(52) Bochicchio, B.; Tamburro, A. M. *Chirality* **2002**, *14*, 782−792.
(53) Eisenhaber, F.; Adzhubei, A. A.; Eisenmenger, F.; Esipova, N. G. *Biofizika* **1992**, *37*, 62−67.
(54) Robin, M. B. *Higher Excited States of Polyatomic Molecules*; Academic Press: New York, 1975; Vol. II.
(55) Song, S.; Asher, S. A. *J. Am. Chem. Soc.* **1989**, *111*, 4295−4305.
(56) Dudik, J. M.; Johnson, C. R.; Asher, S. A. *J. Phys. Chem.* **1985**, *89*, 3805−3814.
(57) Copeland, R. A.; Spiro, T. G. *Biochemistry* **1987**, *26*, 2134−2139.
(58) Mayne, L. C.; Ziegler, L. D.; Hudson, B. *J. Phys. Chem.* **1985**, *89*, 3395−3398.
(59) Mikhonin, A. V.; Bykov, S. V.; Myshakina, N. S.; Asher, S. A. *J. Phys. Chem. B* **2006**, *110*, 1928−1943.
(60) Bykov, S. V.; Lednev, I. K.; Ianoul, A.; Mikhonin, A. V.; Munro, C. H.; Asher, S. A. *Appl. Spectrosc.* **2005**, *59*, 1541−1552.
(61) Mikhonin, A. V.; Ahmed, Z.; Ianoul, A.; Asher, S. A. *J. Phys. Chem. B* **2004**, *108*, 19020−19028.

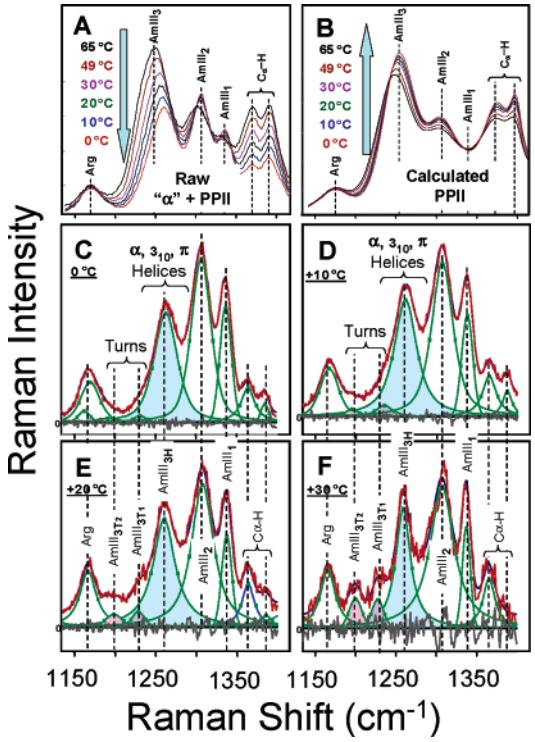

Figure 1. Temperature dependence of the Amide III region of the 204 nm excited UV resonance Raman (UVRR) spectra of AP: (A) experimental spectra; (B) calculated temperature-dependent PPII spectra. Also shown is the temperature dependence of the residual α-helical spectra after removal of the PPII contributions: (C) 0 °C, (D) 10 °C, (E) 20 °C, and (F) 30 °C. The $AmIII_3$ bands of α-helix-like conformations are shown in blue.

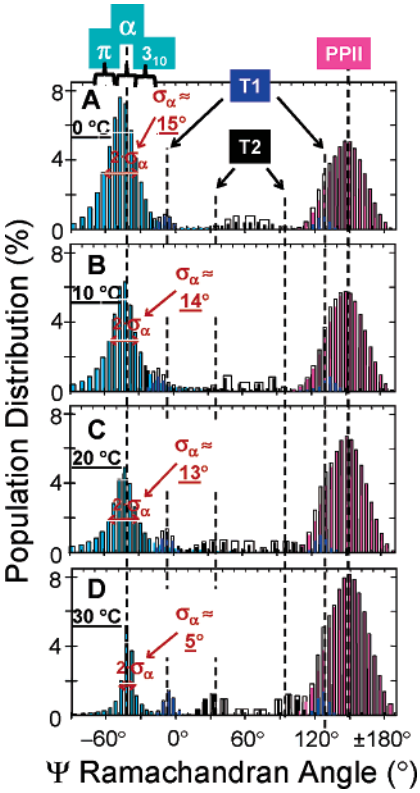

Figure 2. Temperature dependence of the calculated α-helix Ψ Ramachandran angular distributions from the Figure 1C−F AP α-helix UVRR spectra: (A) 0 °C; (B) 10 °C; (C) 20 °C; (D) 30 °C.

The high-temperature Figure 1A spectra and the Figure 1B PPII spectra show a strong $AmIII_3$ band at ∼1245, a minor $AmIII_2$ band at ∼1303, and a ∼1370 and 1394 cm^{-1} doublet from the C_α-H b of the PPII conformation. The Figure 1C−F spectra are α-helix-like. The α-helical spectrum shows an $AmIII_3$ band (which we denote $AmIII_{3H}$) at ∼1261, a ∼1306 $AmIII_2$ band, and a ∼1337 cm^{-1} $AmIII_1$ band. Small bands at ∼1365 and 1387 cm^{-1} may originate either from the CH_3 umbrella mode of ala side chains,[61,62] or derive from C_α-H b of minor turn or β-strand conformations (see later). The band at ∼1165 cm^{-1} originates from the arg side chain,[63] and is useful as an additional internal standard band since its intensity should be independent of temperature.

As shown in detail below, the ∼1228 and ∼1200 cm^{-1} bands (30 °C), which increase in relative intensity with temperature in Figure 1C−F, derive from turn (or β-strand) conformations.[59] Thus, we designate them as $AmIII_{3T1}$ and $AmIII_{3T2}$ bands.

The most striking spectral change with increasing temperature is an ∼2-fold decrease in the $AmIII_{3H}$ peak width with little accompanying change in the relative peak heights. In addition, the relative intensities of the $AmIII_{3T1}$ and $AmIII_{3T2}$ bands increase with temperature. The decreased signal-to noise ratio (S/N) of the higher temperature α-helix spectra (Figure 1E,F) results from the decreased α-helical fractions of AP at 20 and 30 °C, compared to that at lower temperatures.[5,6]

Temperature Dependence of Ψ Ramachandran Angle Distributions of AP. We recently developed a method to determine the peptide bond Ψ Ramachandran angular distributions from the UVRR $AmIII_3$ profiles.[34,38,59,64] Figure 2 shows the temperature dependence of the Ψ angular distributions calculated from the $AmIII_3$ bands of the Figure 1 UVRR spectra of AP.

The Figure 2 Ψ distributions shown in "blue-green" were obtained from the Figure 1C−F $AmIII_{3H}$ band profiles using the following expression developed for the interior α-helix peptide bonds.[59]

$$V_{III3}^{i\alpha}(\psi) = [1244\ cm^{-1} - (54\ cm^{-1}\sin(\psi + 26^0))] \quad (1)$$

where $V_{III3}^{i\alpha}$ is the "α-helical" $AmIII_3$ frequency, which sinusoidally depends on Ψ angle.

The "blue-green" distributions for "α-helical" peptide bonds remain essentially identical between 0 and 20 °C (Figure 2A−C), but begin to narrow and upshift as the temperature increases to 30 °C (Figure 2D). If these distributions are modeled as Gaussians; their average Ψ angle shifts from 48° to 42°, while their bandwidth parameter, σ_α (half width at half-height), narrows from 14.7° ± 3.3° to 5.2° ± 1.4° (Figure 2).

The Figure 2 magenta distributions were calculated from the $AmIII_3$ bands of PPII conformations shown in Figure 1B, using the following expression for peptide bonds fully exposed to water:[59]

$$V_{III3}^{PPII}(\psi,T) = [1256\ cm^{-1} - (54\ cm^{-1}\sin(\psi + 26^0))] - 0.11\frac{cm^{-1}}{°C}(T - T_0)\} \quad (2)$$

(62) Lee, S.-H.; Krimm, S. *Biopolymers* **1998**, *46*, 283−317.
(63) Mikhonin, A. V.; Asher, S. A. *J. Phys. Chem. B* **2005**, *109*, 3047−3052.
(64) Asher, S. A.; Ianoul, A.; Mix, G.; Boyden, M. N.; Karnoup, A.; Diem, M.; Schweitzer-Stenner, R. *J. Am. Chem. Soc.* **2001**, *123*, 11775−11781.

where $V_{III3}^{PPII}(\psi,T)$ is the PPII $AmIII_3$ frequency, T is the experimental temperature, and T_0 is equal to 0 °C.

The Figure 2 Ψ angle distributions shown in blue and black, were calculated from the $AmIII_{T1}$ and $AmIII_{T2}$ bands shown in Figure 1C−F using the average expression for peptide bonds with an unknown hydrogen bonding pattern in water solutions:[59]

$$V_{III3}^{TURNS}(\psi,T) = [1250\ \mathrm{cm}^{-1} - (54\ \mathrm{cm}^{-1}\sin(\psi + 26^0))] - 0.06\frac{\mathrm{cm}^{-1}}{°\mathrm{C}}(T - T_0)\} \quad (3)$$

where all the parameters have the same physical meanings as in the eqs 1 and 2.

Each of the $AmIII_{T1}$ and $AmIII_{T2}$ bands gives two physically possible Ψ angle solutions as shown in Figure 2. The $AmIII_{T1}$ band at ∼1228 cm^{-1} (30 °C) gives a "blue" Ψ distribution which is either centered at Ψ ≈ −5° (which would derive from the $i + 2$ residue of either type I, I′, II, II′ turns[59]), or Ψ ≈ +133° (which would derive from the $i + 1$ residues of type II turns, the $i + 2$ residues of type VIII turns or β-strands[59]). The $AmIII_{T2}$ band at 1200 cm^{-1} (30 °C) has solutions Ψ ≈ +34° (which would derive from the $i + 1$ residue of type I′ or III′ turns, or the $i + 2$ residue of type III′ turns, or from an inverse γ-turn[59]), or Ψ ≈ +94° (which would derive from the $i + 1$ residues of type V turns, and β-strand conformations[59]). We are working on developing a method to determine the Φ angle to discriminate between these conformations.

The relative contribution of these turn (or β-strand) conformations increases as the temperature increases, while the integrated intensity of the broad "α-helix-like" $AmIII_{3H}$ band decreases and its Ψ angle distribution narrows. The intensities of the turn (or β-strand) bands are small, indicating concentrations of less than 7% presuming UVRR cross sections similar to that of the α-helix, or less than 3.5% presuming UVRR cross sections similar to that of PPII.[61]

Simultaneous Existence of α-Helix, 3_{10}-Helix, and π-Helix/Bulge Conformations. The very broad $AmIII_{3H}$ Ψ angle distribution at low temperatures (Figure 2A−C) spans the Ψ angles of the 3_{10}-helix and π-helix/bulge conformations. In contrast, at 30 °C the bandwidth is only ∼50% larger than the homogeneous bandwidth of 7.5 cm^{-1}, which we measured for a small peptide in a single well-defined crystal conformation.[34]

The AP α-helical ensemble at 30 °C is centered at Ψ_{MAX} = −42° with a standard deviation of ±5.2° (Figure 2D). This ±5.2° standard deviation is less than that found in the protein data bank for α-helices in single-crystal proteins.[65] Thus, we conclude that the "α-helix-like" conformation of AP at 30 °C is a pure homogeneous α-helical conformation, while at lower temperatures additional conformations occur. The low Ψ angle standard deviation for the AP pure α-helix conformation presumably results from the high homogeneity of the AP primary sequence.

The 3-fold broader "α-helix-like" Ψ angular distributions (Figure 2A−C, "blue-green" distributions) compared to that at 30 °C (Figure 2D) indicate the presence of additional conformations. We investigated the lower temperature Ψ angular distributions by subtracting the 30 °C pure α-helix distribution from the lower temperature "α-helix-like" distributions. This subtraction is appropriate, because the individual peptide bonds Raman scatter UV light in the AmIII region independently,[63] thus, the resulting UVRR spectra are the linear sums of individual peptide bond contributions. Figure 3, which shows the resulting Ψ angle distributions at 0, 10, and 20 °C, demonstrates two relatively symmetric maxima at approximately −28° and −58°.

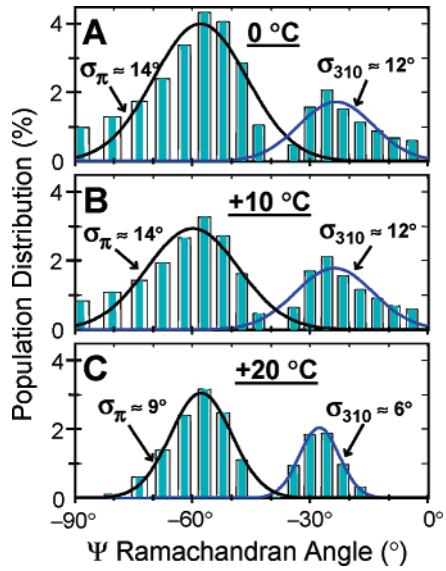

Figure 3. Temperature dependence of Ψ angular distributions for α-helical "defects", calculated by subtracting pure α-helix (Figure 2D) from total (Figure 2A−C) distributions: (A) 0 °C; (B) +10 °C; (C) +20 °C.

The −28° maximum can be directly assigned to 3_{10}-helices (type III turns) which have Ψ and Φ Ramachandran angles of −26° and −60°, respectively. Hydrogen bonding in the 3_{10}-helix occurs between the ith and i + third peptide bonds, making the 3_{10}-helix more tightly coiled than the α-helix. Our observation of 3_{10}-helices agrees with the recent evidence for 3_{10}-helices in ala-rich peptides.[20,23−26,66−81]

The Ψ ≈ −58° distribution most likely originates from π-bulges, which are known to be a common deformation in α-helices.[65] These π-bulges are short intrahelical deformations involving "π-helix-like" hydrogen bonding between the ith and i + fifth residues. Though ideal π-helices show Ψ and Φ Ramachandran angles of −69° and −57°, respectively, π-bulges

(65) Cartailler, J.-P.; Luecke, H. *Structure* **2004**, *12*, 133−144.
(66) Miick, S. M.; Martinez, G. V.; Fiori, W. R.; Todd, A. P.; Millhauser, G. L. *Nature* **1992**, *359*, 653−655.
(67) Fiori, W. R.; Miick, S. M.; Millhauser, G. L. *Biochemistry* **1993**, *32*, 11957−11962.
(68) Millhauser, G. L. *Biochemistry* **1995**, *34*, 3873−3877.
(69) Millhauser, G. L.; Stenland, C. J.; Hanson, P.; Bolin, K. A.; van de Ven, F. J. M. *J. Mol. Biol.* **1997**, *267*, 963−974.
(70) Bolin, K. A.; Millhauser, G. L. *Acc. Chem. Res.* **1999**, *32*, 1027−1033.
(71) Moran, A. M.; Park, S.-M.; Dreyer, J.; Mukamel, S. *J. Chem. Phys.* **2003**, *118*, 3651−3659.
(72) Long, H. W.; Tycko, R. *J. Am. Chem. Soc.* **1998**, *120*, 7039−7048.
(73) Wieczorek, R.; Dannenberg, J. J. *J. Am. Chem. Soc.* **2004**, *126*, 14198−14205.
(74) Hanson, P.; Martinez, G.; Millhauser, G.; Formaggio, F.; Crisma, M.; Toniolo, C.; Vita, C. *J. Am. Chem. Soc.* **1996**, *118*, 271−272.
(75) Hanson, P.; Millhauser, G.; Formaggio, F.; Crisma, M.; Toniolo, C. *J. Am. Chem. Soc.* **1996**, *118*, 7618−7625.
(76) Martinez, G.; Millhauser, G. *J. Struct. Biol.* **1995**, *114*, 23−27.
(77) Silva, R. A.; Gangani, D.; Yasui, S. C.; Kubelka, J.; Formaggio, F.; Crisma, M.; Toniolo, C.; Keiderling, T. A. *Biopolymers* **2002**, *65*, 229−243.
(78) Topol, I. A.; Burt, S. K.; Deretey, E.; Tang, T.-H.; Perczel, A.; Rashin, A.; Csizmadia, I. G. *J. Am. Chem. Soc.* **2001**, *123*, 6054−6060.
(79) Bour, P.; Kubelka, J.; Keiderling, T. A. *Biopolymers* **2002**, *65*, 45−59.
(80) Podtelezhnikov, A. A.; Wild, D. L. *Proteins* **2005**, *61*, 94−104.
(81) Han, W.-G.; Elstner, M.; Jalkanen, K. J.; Frauenheim, T.; Suhai, S. *Intl. J. Quantum Chem.* **2000**, *78*, 459−479.

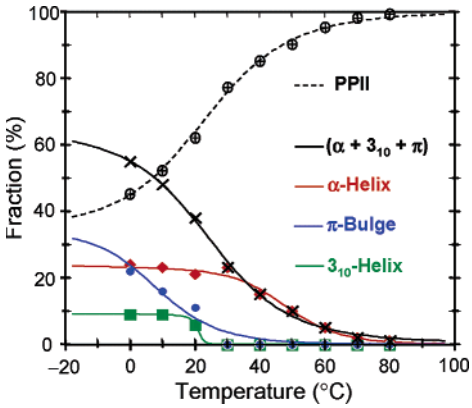

Figure 4. Melting/formation curves for AP major pure secondary structure conformations: (×) original (α-helix" melting curve as reported by Lednev et al.[5,6], which is a sum of individual α− π− and 3_{10}-helical melting curves); (red diamond) perfect α-helix melting; (green square) 3_{10}-helix (type III turn) melting; (blue circle) π-bulge (π-helix) melting; (⊕) PPII formation. The lines through the points for the "α-helix-like" conformations derive from the Zimm−Bragg model as described in the text.

show Ψ angles close to Ψ ≈ −58°. Our observation of π-bulges agrees with recent reports on π-helix/π-bulge conformations in ala-rich peptides.[21,25−27,30,80,82]

We considered the possibility that the Ψ angle distribution assigned to π-bulges instead resulted from the three N-terminal and three C-terminal residues of α-helices which cannot fully intrahelix hydrogen bond. These peptide bonds, which are hydrogen bonded to water, would be frequency upshifted by 9 and 3 cm^{-1}, respectively, compared to those which intrahelix hydrogen bond.[59] However, the high-temperature Figure 2D α-helix distribution indicates that the terminal pure α-helix Ψ angle conformations overlap those of the central α-helix peptide bonds. Thus, we conclude that the terminal residues of the α-helices do not contribute to the Ψ = −58° distribution.

Different Melting Temperatures (T_m) For α-Helix, 3_{10}-Helix, and π-Helix/Bulge. If we assume identical Raman cross sections for the internal and terminal α-helix residues, as well as for the 3_{10}- and π-helices, we can calculate the melting curves for these conformations (Figure 4), as well as the temperature dependence of their Gibbs free energy landscapes (Figure 5). The most striking feature of the Figure 4 melting curves is that α-helix melting now looks more cooperative, with a $T_m \approx 45$ °C, a substantially larger T_m than previously determined by CD[4] and Raman.[5] Melting of the 3_{10}-helices and π-bulges is also cooperative with $T_m \approx 20$ and 10 °C, respectively. Previous studies,[6] unable to distinguish between these conformations, determined a much less cooperative average melting curve which could be well fit by a Zimm and Bragg nucleation parameter, *sig*, of ∼8 × 10^{-4} and a lower T_m = ∼27 °C for the so-called "α-helix". As discussed later, we find that the Figure 4 resolved α-helix melting curve results in quite different Zimm and Bragg nucleation and thermodynamic parameters.

Recently, Ianoul et al.[83] deuterium substituted the penultimate AP residues and demonstrated that the α-helix-like penultimate segments melt at lower temperatures than do the ∼6 central α-helical peptide bonds. This allows us to conclude that the 3_{10}-helices and π-bulge conformations preferentially occur in

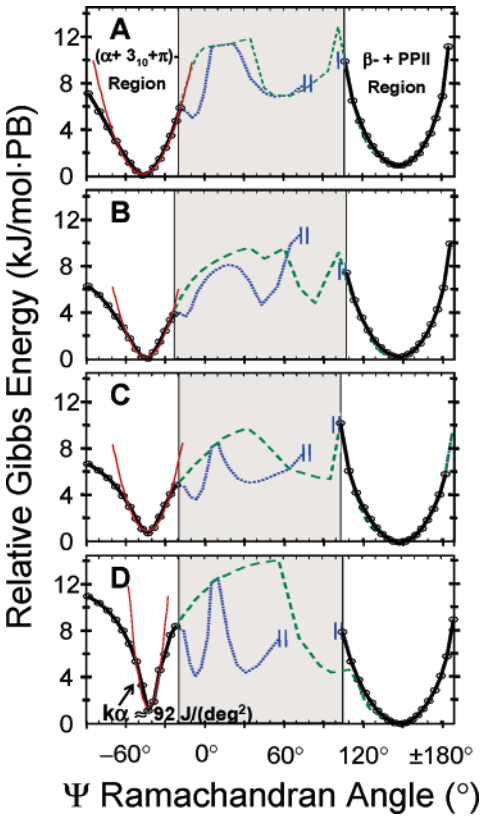

Figure 5. Relative Gibbs energy landscapes (GFEL) for AP at different temperatures: (A) 0 °C, (B) +10 °C, (C) +20 °C, (D) +30 °C. Black lines with circles represent well-determined portions of the GFEL in the α-helix and PPII regions of the Ramachandran plot. The dotted blue line in the uncertain "turn" regions of the Ramachandran plot, assumes that the turns T1 and T2 exist at Ψ ≈ −10° and +30°, respectively. The dashed green line assumes that turns T1 and T2 exist at Ψ ≈ +130° and +90°, respectively. The red line shows the fit of α-helical part of GFEL using the harmonic oscillator approximation. "PB" means "peptide bond".

regions outside the six central AP peptide bonds, toward the ends of the α-helical segments. We can now reconsider the kinetic Raman melting studies of Lednev et al.[6] who measured melting using a *T*-jump from 4 to 26 °C. Figure 4 shows that the π-bulges are the dominant melting species between these temperatures. Thus, we now can conclude that melting of π-bulges occurs with a relaxation time of 180 ± 60 ns at room temperature. If these π-bulges melted to PPII conformations directly in a two-state transition, we would estimate π-bulge folding and unfolding rate constants as 4.0 × 10^5 and 5.2 × 10^6 s^{-1}, respectively.

However, molecular dynamical studies indicate that the 3_{10}-helix and π-bulge conformations are transient α-helix defect structures,[23−27] which are less stable than the pure α-helix conformations and, therefore, melt at lower temperatures. Thus, our estimation of rate constants using a 2-state model is questionable. The stability of 3_{10}-helix and π-bulge conformations derives from the increased peptide bond−water hydrogen bonding stabilization[34,38] that occurs at lower temperatures for the more solvent exposed 3_{10}-helices (type III turns)[84] and π-bulges.[65]

Experimental Gibbs Free Energy Landscapes. We can utilize our calculated conformation population distributions (Figure 2) to calculate portions of the Gibbs free energy

(82) Feig, M.; MacKerell, A. D., Jr.; Brooks, C. L., III. *J. Phys. Chem. B* **2003**, *107*, 2831−2836.
(83) Ianoul, A.; Mikhonin, A.; Lednev, I. K.; Asher, S. A. *J. Phys. Chem. A* **2002**, *106*, 3621−3624.
(84) Sundaralingam, M.; Sekharudu, Y. C. *Science* **1989**, *244*, 1333−1337.

landscape (GFEL) along the Ψ Ramachandran angle folding reaction coordinate, applying the simple Boltzmann argument.[38] Figure 5 shows the resulting AP GFEL at 0, 10, 20, and 30 °C. The black lines through circles show the well-determined portions of the GFEL in the α-helix and the PPII regions of the Ramachandran plot. The red line shows the fit of α-helical part of the GFEL using a harmonic oscillator model $G_\alpha = G_{0\alpha} + k_\alpha(\Psi - \Psi_0)^2/2$. This fit allows us to estimate the torsional restoring force constant (k_α) for a perfect α-helix conformation at 30 °C: $k_\alpha \approx 92$ J/deg^2.

The dotted blue line in Figure 5 shows a very roughly estimated GFEL in the "turn" regions of the Ramachandran plot, assuming that the assigned turns T1 and T2 exist at $\Psi \approx -5°$ and +34°, respectively. In this case, it is not possible to determine the portion of GFEL between Ψ values of ~60° and 100°, nor to reliably determine the free energy barrier between the α-helix and the PPII conformations (60° to 100°, Figure 5). However, we can estimate that the barriers at other angles are <12.5 kJ/(mol·peptide bond) (kJ/(mol·PB)).

The dashed green line in Figure 5 shows another option for the GFEL in the "turn" region of the Ramachandran plot, which assumes that the turns T1 and T2 (or β-strands) exist at $\Psi \approx +133°$ and +94°, respectively. Under this assumption, we estimate that the free energy barriers between the α-helix and PPII conformations lie between 9 and 14 kJ/(mol·PB).

The experimental Figure 5 AP GFELs are qualitatively similar to those theoretically estimated by Young and Brooks[20] for Ace-(Ala)$_n$-NMe (n = 4, 5, 10, 15) in water. However, the Figure 5 GFELs, in addition to pure α-helix and 3_{10}-helix conformations, also include contributions from a π-bulge conformation. It is striking that the Figure 5 activation free energy barriers of ~10 to 12 kJ/(mol·PB) are essentially identical to that of Young and Brooks[20] (~2 to 3 kcal/(mol·PB)). However, we find that the apparent Gibbs free energy difference between the α-helix and 3_{10}-helix conformations is ~2 kJ/(mol·PB), which is smaller than the ~0.6 to 1.6 kcal/(mol·PB) values calculated by Young and Brooks,[20] as well as the ~1 kcal/(mol·PB) calculated value of Tirado-Rives et al.[31]

Applying the similar Boltzmann distribution argument,[38] we can use, for example, the Figure 3C 3_{10}-helix and π-bulge peptide bond distribution to estimate their relative Gibbs free energies, which allows us to determine the torsional constants for the 3_{10}-helix and the π-bulge/helix conformations (Figure 6). We find torsional constants $k_{3_{10}} \approx 146$ and $k_\pi \approx 33$ J/deg^2 for the 3_{10}-helix and the π-bulge at 20 °C, respectively. Thus, the more tightly coiled the "helical" structure, the larger is its torsional force constant ($k_\pi < k_\alpha < k_{3_{10}}$), as expected.

Insights into Complex Melting Kinetics of AP-like Peptides. Our results provide new insights into the melting phenomena of α-helices. The obvious population heterogeneity of the low temperature α-helix-like ensembles should contribute to complicated multiexponential and/or nonexponential kinetics for α-helix melting, which is, in fact, observed for similar peptides.[7,9] This population heterogeneity clarifies why the observed α-helix kinetic melting in these peptides depends on the initial and final temperatures; complicated kinetic behaviors occur for low initial T-jump temperatures,[7,9] whereas at the higher initial sample temperatures, the pure α-helix shows essentially monoexponential kinetic melting.[7,9]

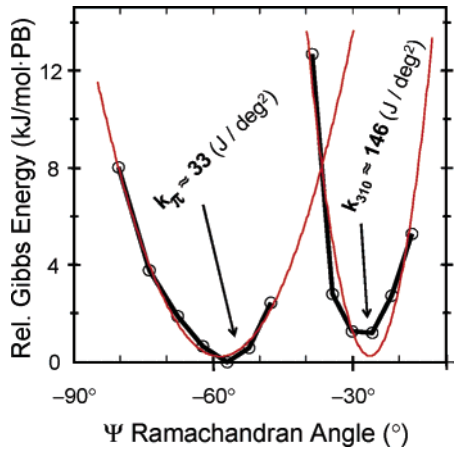

Figure 6. Relative Gibbs free energies of 3_{10}-helix and π-bulge at +20 °C as a function of Ψ angle. Black line through circles shows the calculated GFEL obtained from the Figure 3C distributions. The red line shows the fit of these data points to a harmonic oscillator model. "PB" means "peptide bond".

In addition, the recent kinetic studies of Decatur and co-workers[11,12] suggest that the ala-rich peptides show different monoexponential relaxation times for different isotopically labeled segments of the ala-rich chains, which clearly suggests that the melting of these peptides is not a simple two-state process.

Our melting studies here simply explain the anti-Arrhenius melting kinetics observed by Lednev et al.[5] Folding kinetics are fast at low temperatures where relaxation involves 3_{10}-helices and π-bulges melting to PPII conformations. In contrast, the higher temperature melting T-jumps sampled only pure α-helix melting which was slower. The kinetic measurements were unable at that time to differentiate melting of these different conformations. We describe the origin of this anti-Arrhenius behavior in a forthcoming publication.

Zimm−Bragg Parameters for α-Helix, 3_{10}-Helix, and π-Helix/Bulge Conformations. We can compare the Zimm and Bragg apparent nucleation parameters for these structures and estimate the melting enthalpies and entropies. The system is underdetermined so that these parameters are not independent. Since the perfect α-helix melting is more cooperative than that of the "so-called α-helix" (Figure 4), we will assume that the perfect α-helix $sig_\alpha = \sim 10^{-5}$, somewhat less than the $sig_\alpha = \sim 8 \times 10^{-4}$ reported by Lednev et al.[6] The entropic cost for forming the first hydrogen bond in 3_{10}- and α-helices is counted in the nucleation parameter, sig. Sheinerman and Brooks[85] argued that two additional dihedral angles must be restricted to initially form a 3_{10}-helical turn, while four additional dihedral angles must be restricted to initially form an α-helical turn. This led them to estimate that the nucleation parameter for the 3_{10}-helix is $sig_{3_{10}} \approx (sig_\alpha)^{0.5}$. Applying this argument to a π-bulge we estimate that $sig_\pi \approx (sig_\alpha)^{1.5}$, since six additional dihedral angles must be restricted to form first π-helical turn. Thus, taking $sig_\alpha \approx 10^{-5}$, we estimate $sig_{3_{10}} \approx 3 \times 10^{-3}$ and $sig_\pi \approx 3 \times 10^{-8}$. This approach allows for an adequate fit to the observed melting curves for perfect α-helices and π-helices/bulges (Figure 4). We find hydrogen bonding enthalpies of $\Delta H = -7.2$ and −4.4 kJ/(mol·res) for the perfect α-helix and the π-helix/bulge,

(85) Sheinerman, F. B.; Brooks, C. L., III. *J. Am. Chem. Soc.* **1995**, *117*, 10098−10103.

respectively. We also estimate entropies $\Delta S = -17.4$ and -7.8 J/(mol•K•res) for the perfect α-helix and π-helix/bulge, respectively. In contrast, the Zimm and Bragg model fails to adequately describe the melting of 3_{10}-helices with physically reasonable nucleation and propagation parameters σg and s, although it is possible to get an adequate fit (Figure 4).

Alternatively we can constrain the enthalpy for all these structures to be -6.3 kJ/(mol•res) and then estimate the nucleation parameters and the entropies. This approach provides the nucleation parameters of $\sim 1 \times 10^{-7}$, 1×10^{-8}, and 1×10^{-5}, for α-helix, 3_{10}-helix, and π-helix/bulge, respectively. We also estimate entropies of approximately -7.9, -7.8, and -14.6 J/(mol•K•res), respectively. Assuming the same enthalpies we find that the nucleation parameters follow a trend, exactly opposite of that expected by Sheinerman and Brooks.[85] Whatever the case, the melting of α-helix-like AP is definitely far from a two state transition. Thus, the physical meaning of these Zimm and Bragg parameters is no longer straightforward.

Concusions

Our ability to directly monitor the Ψ Ramachandran angles of peptide bonds allows us for the first time to separately study the melting of the α-, 3_{10}-, and π-helix/bulge conformations. It is somewhat surprising to find that the 3_{10}- and π-helix/bulge conformations melt prior to melting of pure α-helices, since these conformations are proposed to be intermediates in the unfolding pathway. Apparently they are much more transient at the higher α-helix melting temperature.

We estimated Zimm and Bragg nucleation (σg) and propagation (s) parameters for perfect α-helix and π-helix/bulge conformations. A striking finding is that the AP pure α-helix melts with much higher cooperativity and shows much higher T_m, ~45 °C, then was originally reported by CD[4] and Raman.[5] We were able for the first time to experimentally monitor the Gibbs free energy landscapes and the free energy barriers on the AP melting reaction pathway. These experimental measurements should serve as a benchmark for theoretical studies of protein folding. Future equilibrium and kinetic studies of isotopically edited peptides will allow us to more deeply examine "α-helix" to PPII melting, as well as other peptide backbone conformational transitions.

Acknowledgment. The authors are very grateful to NIH (Grant GM8RO1EB002053-24) for financial support. We also thank Zeeshan Ahmed, Dr. Nataliya Myshakina, and Dr. John Scaffidi for useful discussions.

JA062269+